

Non-Markovian decay and dynamics of decoherence in private and public environments

A. D. Dente, P. R. Zangara, and H. M. Pastawski*

Instituto de Física Enrique Gaviola (CONICET) and Facultad de Matemática, Astronomía y Física, Universidad Nacional de Córdoba, Ciudad Universitaria, 5000, Córdoba, Argentina

We study the decay process in an open system, emphasizing on the relevance of the environment's spectral structure. Non-Markovian effects are included to quantitatively analyze the degradation rate of the coherent evolution. The way in which a two level system is coupled to different environments is specifically addressed: multiple connections to a single bath (public environment) or single connections to multiple baths (private environments). We numerically evaluate the decay rate of a local excitation by using the Survival Probability and the Loschmidt Echo. These rates are compared to analytical results obtained from the standard Fermi Golden Rule (FGR) in Wide Band Approximation, and a Self-Consistent evaluation that accounts for the bath's memory in cases where an exact analytical solution is possible. We observe that the correlations appearing in a public bath introduce further deviations from the FGR as compared with a private bath.

PACS numbers: 03.65.Yz, 03.65.Ta, 03.67.Pp

arXiv:1106.2457v2 [quant-ph] 31 Aug 2011

* horacio@famaf.unc.edu.ar

I. INTRODUCTION

Quantum Information Processing (QIP) requires an efficient and precise control on quantum dynamics [1]. Decoherence conspires against this objective as it leads to progressive and smooth destruction of the quantum interferences [2] within a characteristic time τ_ϕ . The main source of decoherence for solid-state spin systems such as quantum dots [3–6], donors in silicon [7], defects in diamond [8–10], and solid state nuclear magnetic resonance (NMR) [11–13] is the uncontrolled spin bath environment. While one can attempt different strategies such as quantum error correction protocols [14, 15] and dynamical decoupling [16], their specific efficiency depends on a deep understanding of how the environment behaves. Thus, understanding and mitigation of decoherence is one of the current challenges for quantum science and technology [17–19].

The interaction rate $1/\tau_{\mathcal{S}-\mathcal{E}}$ between a quantum system \mathcal{S} and its environment \mathcal{E} is typically evaluated from a Fermi Golden Rule (FGR), which assumes that the environment has a Markovian nature. Also, the interplay between the system time scales (e.g. $1/\omega_0$) and that of the interaction ($\tau_{\mathcal{S}-\mathcal{E}}$) could result in striking effects. While weak interactions ($1/\tau_{\mathcal{S}-\mathcal{E}} \ll 2\omega_0$) simply degrade dynamical interferences at a rate $1/\tau_\phi \propto 1/\tau_{\mathcal{S}-\mathcal{E}}$, stronger ones may change the system’s response radically, leading to a quantum dynamical phase transition in its dependence on $1/\tau_{\mathcal{S}-\mathcal{E}}$ [13]. Indeed, the possibility of a non-analytic behavior, e.g. in the energy spectrum [20], appears because the system’s effective Hamiltonian is non-Hermitian [21, 22]. This, in turn, can be traced back to the fact that the environment has a number of degrees of freedom N which can be considered infinite. As P.W. Anderson put forth: “more is different”, and new physical phenomena may appear when this thermodynamic limit ($N \rightarrow \infty$) is properly taken [23]. Indeed, there are several models of both non-Markovian and Markovian environments [22, 24–26] which show this dynamical phase transition as a function of the interaction strength.

While the Markovian approximation is sufficient for most traditional applications, it leaves aside important memory effects and interferences in the time domain. These result from the coherent interaction between \mathcal{S} and \mathcal{E} , and are becoming a topic of increasing interest [27]. The system-environment dynamics may go through different temporal regimes: a quadratic decay at very short times yields to the usual exponential FGR decay and much later it is transformed into an inverse power law decay (see Ref. [28]). Here, we will focus on the more relevant exponential regime, treated both with the FGR and with a Self-Consistent (SC) FGR which accounts for bath memory effects. Once again, a deep understanding of the environment’s dynamics is central to identify the different regimes and to foresee possible dynamical transitions.

A natural way to quantify the decoherence time τ_ϕ is through the degradation of specific interferences, e.g. Rabi oscillations [29, 30] or mesoscopic echoes [31–34]. Alternatively, the implementation of a time reversal procedure, the Loschmidt Echo (LE) [35], allows the evaluation of the decoherence time by measuring the reversibility of the system’s dynamics in presence of an uncontrolled environment. The LE can be accessed experimentally in spin systems [36, 37], confined atoms [38], microwave excitations [39], etc., and has become a powerful tool for quantifying decoherence, stability and complexity in dynamical processes in several physical situations [40, 41].

In this article we have the aim to quantify the role of bath’s memory as well as specific correlations in the $\mathcal{S} - \mathcal{E}$ interaction on decoherence. With this purpose, we consider the evolution of two coupled spins in the $\uparrow\downarrow$ and $\downarrow\uparrow$ configurations in the presence of different spin environments with a fully characterized coherent dynamics [42]. The system’s Rabi oscillations [43] can act as a SWAP gate, and after appropriate mappings, this boils down to an excitation that jumps between two degenerate states A and B with a rate determined by the coupling “constant” V_{AB} , which can be switched at will. Starting on state A , the return probability oscillates with $\omega_0 = 2V_{AB}/\hbar$, the Rabi frequency. In order to understand the incidence of environmental memory effects in the rate $1/\tau_\phi$, we must consider the relation between the system’s time scale (typically ruled by \hbar/V_{AB}) and the bath’s inner excitation spreading time scale as determined by the density of directly connected states $\hbar N_1$, which, in general, is just a Local Density of States (LDoS) [44]. Also important is the specific form in which the system couples to the bath: each site may be coupled to a different environment (private bath) or both sites could share the same environment (public bath), and this would allow different correlations. A quantitative comparison between rates in these cases will enable a qualitative interpretation in terms of the bath’s spectral structure and the effects of public and private $\mathcal{S} - \mathcal{E}$ interactions. This should deepen our understanding about how the involved correlations modify the degradation rate $1/\tau_\phi$. Indeed, if the system’s and the bath’s time scales are similar, the problem cannot be treated within the Markovian paradigm of a “slow variable interacting with a fast equilibrating background”. It requires to be carefully addressed beyond the FGR. The appearance of mechanisms of correlated coupling in public environments has been previously pointed in the literature of open quantum systems, particularly in terms of the spin-boson models [45, 46]. It was shown [46], at least for a simple model of a N -qubit register, that the decoherence increases linearly with N for independent reservoirs, while it grows with the square N^2 for a collective environment. This suggests that such a public interaction may lead to a strong amplification of decoherence. On the other hand, it has been pointed in the literature of error correction protocols that symmetric (public) $\mathcal{S} - \mathcal{E}$ coupling can be exploited to design states that are hardly corrupted by such a coherent environmental noise [47]. Also, in recent years the role of a common environment in the

entanglement correlations within a system [48, 49], and the possibility of creating and manipulating those correlations by environment-mediated interactions [50] have been explored.

It is important to notice that spectral correlations within the bath, as described above, may become quite cumbersome to describe in statistical terms. However, realistic Hamiltonian models of the bath, as proposed here, should allow a simple and natural description of such correlations. Thus, the cases we analyze here can be casted directly into 1-D spin systems interacting by means of a planar (XY or flip-flop) or as chains of spins interacting with a double-quantum (flip-flip / flop-flop) effective Hamiltonians. Indeed, the spin-fermion mapping provided by the Jordan-Wigner Transformation (JWT) [51] has been successfully exploited to predict spin polarization dynamics in linear chains and rings [33] and results in full agreement with experiments [31, 34]. Furthermore, it allowed addressing polarization spin dynamics in homogeneous chains [28, 30, 52] and dynamics of multiple spin coherences [53–56] by mapping them to fermionic excitations. In both cases, the local excitation is identified with a single fermion propagating in a tight-binding linear chain, and one can assume that the environment is described by an identical chain. Additionally, the dynamics of a tight-binding model can be mapped, sometimes quite straightforwardly, to describe the propagation of excitations in several scenarios like classical and quantum coupled oscillators [57], plasmonic wave guides [58], sound propagation [59], spin-boson interactions and other models used for decoherence in quantum information [60, 61].

A fundamental issue about integrability of the chosen models is that they enable analytical expressions valid in the thermodynamic limit of an infinite number of spins. In fact, an analytically tractable bath means the capability to sum up an otherwise divergent perturbation series into a complex self-energy through the Dyson Equation, which only then is considered in the FGR approximation. Additionally, having a smooth LDoS, which arises from a continuous spectrum ($N \rightarrow \infty$), avoids spurious resonances that might appear in finite systems. Besides, we will see that a well defined curvature of the LDoS will be central to quantify the corrections to the FGR.

This paper is organized as follows. In Sec. II we present the $\mathcal{S} - \mathcal{E}$ tight-binding models that yields a fully solvable quantum dynamics (the underlying spin-fermion mapping is summarized in the Appendix A). In Sec. III, the notions of Survival Probability and local Loschmidt Echo are presented on the face of their numerical implementation. We deal analytically with every case by working with the exact Green's Function in each case. Further details related to the GF's poles are discussed in Appendix B. In Sec. IV, the analytical decay rates obtained with the FGR and the SC-FGR are presented for each case under consideration. These rates are compared with those computed numerically from the dynamics, contrasting the results of the Survival Probability (SP) and the Loschmidt Echo (LE) of the local excitation. All these magnitudes are analyzed under the light of the knowledge of the environment memory effects as provided by its spectral structure (LDoS). In the last section, further discussions and conclusions are presented to argue how the public bath is more effective to distort the decay process away from the usual Fermi Golden Rule (energy independent rate).

II. TIGHT BINDING MODEL FOR EXCITATION DYNAMICS

As pointed above, while our motivation lies mainly on spin dynamics under flip-flop interactions, we use the spin-fermion mapping to cast it in terms of tight-binding models that apply to a wide variety of systems. Thus, we leave to Appendix A a brief outline of how this mapping is achieved. Here, we present the models and analyze them in terms of straightforward single particle physics. These are basically variations of tight-binding infinite linear chains where the bath's memory can be fully characterized. Of course, the cases where the interactions network topology has branching points or loops would preclude the simple back transformation into spin systems. However, even in these situations some of the physics of the memory would remain. The general situations are sketched in Fig.1.

For the cases considered in this article, the whole Hamiltonian can be written as:

$$\hat{H} = \hat{H}_S + \sum_{\nu} \hat{H}_{\mathcal{E}_{\nu}} + \hat{H}_{S-\mathcal{E}}, \quad (1)$$

where:

$$\hat{H}_S = E_A \hat{c}_A^{\dagger} \hat{c}_A + E_B \hat{c}_B^{\dagger} \hat{c}_B - V_{AB} (\hat{c}_A^{\dagger} \hat{c}_B + \hat{c}_B^{\dagger} \hat{c}_A), \quad (2)$$

with \hat{c}_s^{\dagger} and \hat{c}_s ($s \in \{A, B\}$), the creation and destruction operators for fermions and V_{AB} is the hopping amplitude that defines the system's only dynamical time scale provided that $E_A = E_B$. Each bath \mathcal{E}_{ν} ($\nu=1,2$), with a spectral bandwidth of $4V$, is described by the Hamiltonian:

$$\hat{H}_{\mathcal{E}_{\nu}} = \sum_{n=n_{\nu}}^{\infty} E_{\nu n} \hat{c}_{\nu n}^{\dagger} \hat{c}_{\nu n} - V (\hat{c}_{\nu, n+1}^{\dagger} \hat{c}_{\nu, n} + \hat{c}_{\nu n}^{\dagger} \hat{c}_{\nu, n+1}). \quad (3)$$

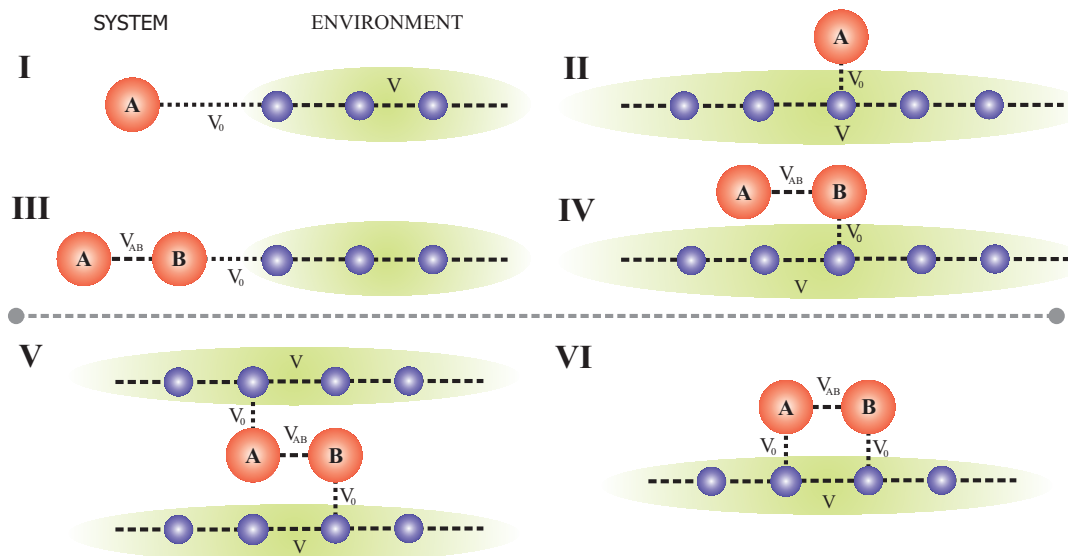


FIG. 1. (Color Online) Non interacting fermion modelization. **I**) A single site state connected to a semi infinite chain. **II**) One site coupled to an infinite chain. Since $V_0 \ll V$, both cases can be treated by a simple decay process, given by the FGR. **III**) Two sites; the initial configuration is given by a particle in the site **A**. The sites are coupled to a semi infinite chain by only one of them. **IV**) Same as **III**), but with an infinite linear chain standing for the bath. **V**) Two sites coupled both to different infinite chains (private environments). **VI**) Two sites coupled to the same infinite chain (public environment).

Choosing the site energies with identical values: $E_{\nu,n} = 0$ ensures a continuum spectrum, while the election $E_A = E_B = 0$ will further simplify the analysis. Two different alternatives for the spectrum dynamics arise when $n_\nu = 1$ (semi-infinite linear chain) and $n_\nu = -\infty$ (infinite linear chain). The system-bath Hamiltonian $\hat{H}_{S-\mathcal{E}}$ depends on how we couple our two-site system to the environment (linear chain), but in general it will be of the form:

$$\hat{H}_{S-\mathcal{E}} = -V_0 \left(\hat{c}_A^\dagger \hat{c}_{\nu i} + \hat{c}_{\nu i}^\dagger \hat{c}_A + \hat{c}_B^\dagger \hat{c}_{\mu j} + \hat{c}_{\mu j}^\dagger \hat{c}_B \right), \quad (4)$$

where νi and μj label sites i and j in the environments ν and μ respectively.

It is crucial to stress that V_{AB} , V_0 and V determine the relevant time scales of the whole problem. The first two give the rate of hopping from site A to site B and to the environment, respectively. The third is the jumping rate between sites in the environment. An “irreversible” decay to the environment, and hence the Fermi Golden Rule, implies that the unperturbed isolated system state has zero overlap with eigenstates of $\mathcal{S} + \mathcal{E}$. For this perturbation theory break down, the interaction with each environment eigenstate, V_0/\sqrt{N} must be much greater than the spacing between adjacent levels, of about V/N , i.e. the interaction time scale \hbar/V_0 must be lower than the environment’s Heisenberg time $\hbar N/V$. Imposing $V_0 \ll V_{AB}$ for all the cases we treated (weak coupling regime), we ensure the smooth degradation of the system’s coherent evolution. When $V \approx V_{AB}$ the memory effects characterizing a *non-Markovian* situation lead to a very rich dynamical behavior. In the opposite limit, if $V \gg V_{AB}$ then the validity of the FGR (*Markovian* situation) is expected to be recovered. Typically, this last situation will be represented in this work by a hopping $V = 5V_{AB}$.

III. NUMERICAL AND ANALYTICAL TOOLS

A. SURVIVAL PROBABILITY AND LOSCHMIDT ECHO

Two kind of measures for dynamical degradation are employed in this work: the Survival Probability (SP) $P_{AA}(t)$ and the local Loschmidt Echo. The SP is defined as

$$P_{A,A}(t) = \left| \langle A | \exp \left[-i\hat{H}t/\hbar \right] | A \rangle \Theta(t) \right|^2, \quad (5)$$

where $\Theta(t)$ is the Heaviside step function, and the Hamiltonian \hat{H} is defined by Eq. 1. It measures the probability of finding a particle in site A at time t , provided that the system has had a particle in the same site at time $t = 0$. In spin systems, this is a spin autocorrelation function (see Eq. A3 and A6 in Appendix A). The whole evolution of the system as reflected in the SP, is affected by a decay process, which is not trivial to separate from the intrinsic dynamics. Thus, to quantify decoherence, one relies on the observation of specific features as natural recurrences (Rabi oscillations or mesoscopic echoes) that appear at specific times. This limits the used time windows and limits the detailed assessment of $\mathcal{S} - \mathcal{E}$ dynamics. Although it is not the perfect tool to quantify the effects of the environment, the SP behaves as a probe that reflects the overall dynamical process.

With the purpose of get a continuous access to the $\mathcal{S} - \mathcal{E}$ dynamics that better reflects the environmental memory effects, we focus our attention on the LE. This measure has been used in the last years in different physical scenarios (both experimental [36–39] and theoretical [35, 40, 62]) in order to explain the behavior of the decoherence characteristic time. In general, the LE provides a direct measure of the decoherence process due to the environment, and even though it depends on the nature of the system’s intrinsic dynamics, it does not depend much on its details. Its usual dynamical behavior presents an exponential decay regime [63], which will be used to characterize the destruction of the system’s coherent dynamics.

The LE relies on the time reversal of the system’s evolution and, in the present scenario, it has a direct physical interpretation. The LE can be understood as the measure of the amount of polarization returned to *local* site where it started. The controlled quantum dynamics is separated in two stages. First, the initial local excitation (particle in site A) evolves during a time t_1 , and then a time reversal procedure is applied during a period time $(T - t_1)$ which reverses the system’s dynamics ($\hat{H}_{\mathcal{S}} \rightarrow -\hat{H}_{\mathcal{S}}$). It is important to note that the bath’s dynamics and the $\mathcal{S} - \mathcal{E}$ interactions ($\hat{H}_{\mathcal{E}}$ and $\hat{H}_{\mathcal{S}-\mathcal{E}}$ respectively) remain unreversed during the backward evolution. This partial control results in a non-reversed perturbation $\hat{\Sigma} = (\hat{H}_{\mathcal{E}} + \hat{H}_{\mathcal{S}-\mathcal{E}})$ acting in both periods. Finally, the probability of finding the particle in site A forms a Loschmidt echo provided that $t_1 = T/2$:

$$M_{LE}(T) = \left| \langle A | \exp \left[-i(-\hat{H}_{\mathcal{S}} + \hat{\Sigma})(T - t_1)/\hbar \right] \exp \left[-i(\hat{H}_{\mathcal{S}} + \hat{\Sigma})t_1/\hbar \right] | A \rangle \right|^2. \quad (6)$$

Clearly, in the case where the system is isolated, the local LE will have a steady value of 1. This means that the system is fully reversible. On the other hand, if the system is coupled to the infinite and continuous environment’s spectrum, both the forward and backward effective Hamiltonians, $\hat{H}_{\mathcal{S}} + \hat{\Sigma}$ and $-\hat{H}_{\mathcal{S}} + \hat{\Sigma}$ respectively, become non-Hermitian. Thus, the LE decays with a characteristic rate, i.e., our reversal procedure has not been able to recover the excitation spread to the environment. The net decay of the norm of the state simply means the decay of the coherent part and then describes the non-trivial part of the Loschmidt Echo.

For both survival probability and Loschmidt Echo evaluation, we diagonalize the Hamiltonian to obtain the evolution for every time. We use sufficiently large chains to approximate the nature of infinite ones. Indeed, the evolution times considered in this work are short enough to ensure the absence of dynamical finite-size effects (e.g. mesoscopic echoes appearing at the environment’s Heisenberg time). A typical system is presented in Fig. 2-a (the same model was deeply analyzed in Ref. [42]).

We are interested in studying the decay rates as a function of the $\mathcal{S} - \mathcal{E}$ coupling parameter V_0 (from Hamiltonian of Eq. 4). We fit the dynamics of the local LE with exponential decay function, which for the case plotted in Fig. 2-b, turns out to be the envelope of the Rabi oscillations in the SP and has the advantage of having a monotonous behavior. However, one should be aware that for an arbitrary system, the SP envelope does not necessarily match the local LE (the characteristic rates can be different). Every rate we obtain, is related to a particular choice of V_0 , and we want to use them to asses the conditions of validity of a FGR regime:

$$\frac{1}{\tau_{\phi}} \simeq \frac{2\pi}{\hbar} \left(\hat{H}_{\mathcal{S}-\mathcal{E}} \right)^2 N_1, \quad (7)$$

where $\left(\hat{H}_{\mathcal{S}-\mathcal{E}} \right)^2$ is a characteristic second moment of the $\mathcal{S} - \mathcal{E}$ interaction and N_1 represents an appropriate density of directly connected states. Thus, we plot the decay rates as a function of $V_0^2/\hbar V$ (Fig. 2-c). It is interesting to note that because of the linear chain topology this second moment coincides with V_0^2 and N_1 can be identified with a local density of state at the first site of the chain. In a general environment this correspondence can be assigned through a Lanczos transformation [44].

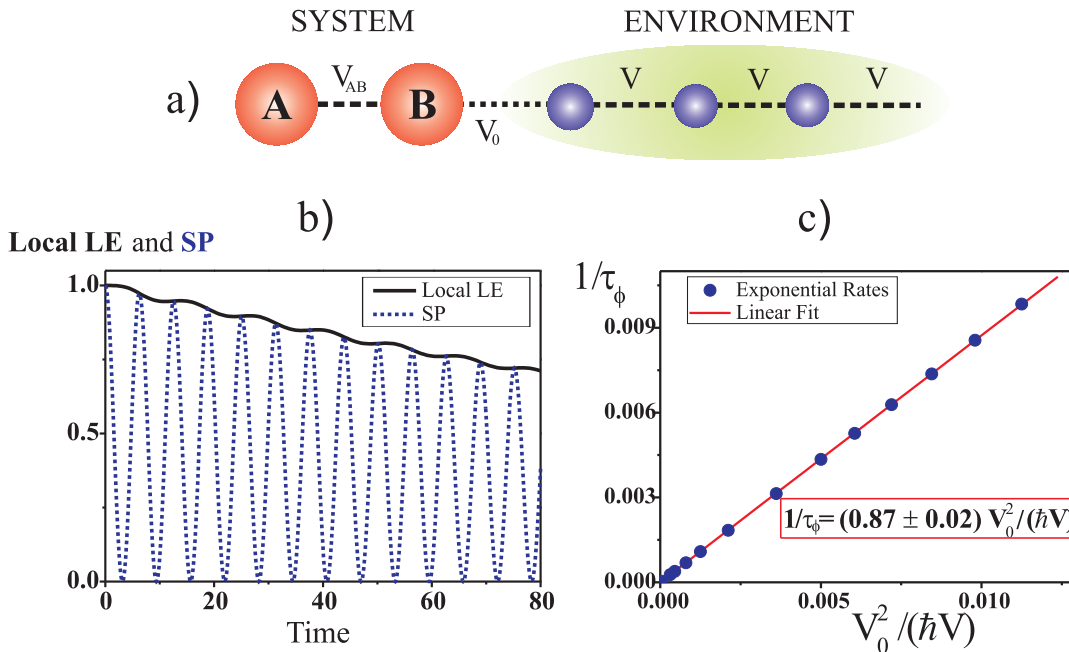


FIG. 2. (Color Online) **a)** Typical tight binding model considered. **b)** SP (dotted line) and the local LE (solid line) plots vs. time (in units of \hbar/V_{AB}). **c)** Characteristic decay rate (exponential decay regime) as a function of $V_0^2/\hbar V$ (both in units of V_{AB}/\hbar). The points were obtained by the variation of the coupling constant V_0 .

B. ENVIRONMENT'S EFFECT IN A SELF-CONSISTENT FERMI GOLDEN RULE

For the study of the analytical solutions we use the Green's Function (GF) formalism. In this framework it is possible to obtain the overall dynamics of the system by looking at the behavior of the GF poles [28, 42]. Any element of the retarded GF can be obtained from the Fourier transform of the full propagator:

$$\begin{aligned}
 G_{AA}^R(\varepsilon) &= \lim_{\eta \rightarrow 0} \int_{-\infty}^{\infty} \langle A | \exp \left[-i \left(\hat{H} - i\eta \hat{I} \right) t / \hbar \right] | A \rangle \Theta(t) \exp [+i\varepsilon t / \hbar] dt \\
 &= \frac{1}{\varepsilon - E_A - \Sigma(\varepsilon)} = \frac{1}{\varepsilon - E_A - \Delta(\varepsilon) + i\Gamma(\varepsilon)},
 \end{aligned} \tag{8}$$

where $\Sigma(\varepsilon)$ is the appropriate self-energy with real and imaginary parts $\Delta(\varepsilon)$ and $-\Gamma(\varepsilon)$ respectively. The self-energy operator is diagrammatically presented in Fig. 3. The bath memory is contained in their dependence on ε , which arises from the bath's exact Green's Function $\overline{G}_{11}^R(\varepsilon)$ at the directly connected site. Indeed, $\Sigma(\varepsilon)$ is given by $|V_0|^2 \overline{G}_{11}^R(\varepsilon)$, see Fig. 3-b. All the cases considered in this work (see Fig. 1) can be reduced to the self-energy of a semi infinite linear chain ($n_\nu = 1$), i.e.

$$\Sigma(\varepsilon) = \frac{V_0^2}{V^2} \left[\frac{\varepsilon}{2} - i\sqrt{V^2 - \left(\frac{\varepsilon}{2}\right)^2} \right] \text{ for } |\varepsilon| \leq 2|V|. \tag{9}$$

For the infinite linear case ($n_\nu = -\infty$), the previous expressions must be multiplied by 2.

Notice that $\Sigma(\varepsilon)$ plays the role of the influence functional in the Feynman path integral formulation usually used to deal with memory effects for bosonic baths [64]. However, in such cases there are many more free parameters than in our case, i.e. the bath spectral density, the coupling strength with each mode and the temperature that fixes the bath occupation. In our spin environment model however, the last is simplified by the high temperature limit, while the two first become naturally determined by specific sum rules arising from the physical Hamiltonian we select.

We remark that the complex GF poles are consequence of the unbounded nature of the system which prevents mesoscopic echoes [33] and Poincaré's recurrences. Also it is important to point out that we are working with a Hamiltonian in a parametric region holding a continuous spectrum where no localized modes appear.

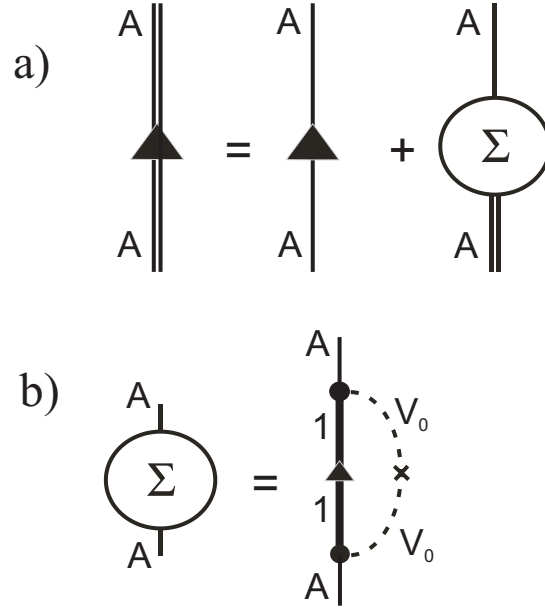


FIG. 3. **a)** Diagrammatic representation for the retarded GF at site A , in the form of a Dyson's equation. The interaction with the environment is to infinite order in the self-energy given in **(b)** (see Eq. 8). Simple lines with arrows are exact GF in absence of $\mathcal{S} - \mathcal{E}$ interactions. **b)** Self-energy diagram sums all orders in the hopping to the environment. Thick line with arrows is the exact propagator at a point of the isolated bath, denoted by \overline{G}_{11}^R (see text).

To get a better understanding of the connection between the dynamical behavior and the poles of the GF, we span the initial condition in the Survival Probability (see Eq. 5) in terms of the energy eigenstates:

$$\begin{aligned}
 P_{AA}(t) &= \left| \Theta(t) \sum_{k=1}^{\infty} |\langle \psi_k | A \rangle|^2 \exp[-i\varepsilon_k t / \hbar] \right|^2 \\
 &= \left| \Theta(t) \int_{-\infty}^{\infty} d\varepsilon \left[\sum_{k=1}^{\infty} |\langle \psi_k | A \rangle|^2 \delta(\varepsilon - \varepsilon_k) \right] \exp[-i\varepsilon t / \hbar] \right|^2.
 \end{aligned} \tag{10}$$

The term in brackets is identified as the Local Density of States (LDoS) $N_A(\varepsilon)$ at the site A :

$$\begin{aligned}
 N_A(\varepsilon) &= -\frac{1}{\pi} \text{Im} \int_{-\infty}^{\infty} dt G_{AA}^R(t) \exp[-i\varepsilon t / \hbar] \\
 &= -\frac{1}{\pi} \text{Im} G_{AA}^R(\varepsilon).
 \end{aligned} \tag{11}$$

Therefore, we can identify Eq. 5 as the LDoS Fourier transform:

$$P_{A,A}(t) = \left| \Theta(t) \int_{-\infty}^{\infty} \frac{d\varepsilon}{2\pi\hbar} N_A(\varepsilon) \exp[-i\varepsilon t / \hbar] \right|^2. \tag{12}$$

The last expression can be numerically and analytically computed once we know the GF in the energy representation. As a matter of fact, since we have $\Sigma(\varepsilon)$, and hence $N_A(\varepsilon)$, explicitly, we can compute the dynamics from the Fourier Transform mentioned. But, we preferred to obtain the numerical evolution (by exact diagonalization, as explained in previous section) of a finite environment. The interest in this last method arises from the fact that its use can be directly generalized to more complex systems (many-body), where an exact analytical solution is not accessible. The

analytical alternative based on the evaluation of the GF poles will enable to summarize the decay rate in a simple expression, as it is shown below.

The characteristic decay of $P_{A,A}(t)$ is determined by the bath's LDoS, $N_1(\varepsilon)$. This last can be obtained from the isolated bath's exact GF at site 1 (i.e. \overline{G}_{11}^R),

$$N_1(\varepsilon) = -\frac{1}{\pi} \text{Im} \overline{G}_{11}^R(\varepsilon). \quad (13)$$

Hence, we recall that $N_1(\varepsilon)$ plays the most relevant role in $\mathcal{S} - \mathcal{E}$ dynamics as was quoted in Ref. [42]. In some systems the LDoS can be factorized as $N_A(\varepsilon) = N_1(\varepsilon) \times L_1(\varepsilon) \times L_2(\varepsilon)$, where $L_i(\varepsilon)$ are Lorentzian functions (LFs) related to the real and imaginary parts (denoted by Δ_0 and Γ_0 respectively) of the GF poles. Hence, the convolution theorem applied to Eq. 12 leads to a characteristic decay of $P_{A,A}(t)$ ruled by Γ_0 . In fact, the decay parameter of the exponential regime is given by $1/\tau = 2\Gamma_0/\hbar$. This is what we call self-consistent Fermi Golden Rule (SC-FGR) [28].

With the purpose of finding Γ_0 , we focus on the Hamiltonian 1, and follow the continued-fraction procedure described in Ref. [65]. For each type of $\mathcal{S} - \mathcal{E}$ coupling (see Fig. 1), it is necessary to recalculate the poles of the GF. Due to the small number of poles of the systems, it was feasible to obtain the analytical solutions for all the cases presented in this work. Also, we address the behavior of Γ_0 as a function of $V_0 \ll 1$. Indeed, we proceed to expand the solution near $V_0 \simeq 0$.

It is important to notice that in the Taylor expansion, the linear and zero order terms vanish. Therefore, the imaginary part has V_0^2 as the first non trivial term. As expected for a FGR, this is in strong agreement with Eq. 7, where we identify the order V_0^2 as the second moment of the $\mathcal{S} - \mathcal{E}$ interaction (in general denoted by $\left\| \hat{H}_{\mathcal{S}-\mathcal{E}} \right\|^2$). In the next section, we present the corresponding values for $1/\tau = 2\Gamma_0/\hbar$, expressed in the first non trivial order (as we said, the 2nd), for each case considered.

The usual alternative (easier and cheaper) to the presented scheme (SC-FGR) is the simple FGR, which is equivalent to evaluate the Green's function in a first pole approximation:

$$[G_{AA}^R(\varepsilon)]^{-1} \simeq \varepsilon - E_A - \Sigma(E_A) \quad (14)$$

$$= \varepsilon - E_A - \Delta(E_A) + i\Gamma(E_A) \quad (15)$$

Since this yields an ε -independent rate, it can be understood as a Wide Band Approximation (WBA) [66–68]. This approximation would imply neglecting any signature of dynamics and memory effects in the environment. Also, it misses some striking dynamical behaviors appearing at long times as the survival collapse [28, 42] and the subsequent power law decay [69–71].

As a matter of fact, the WBA is represented by the condition of $V \gg V_{AB}$. Under this assumption, the environment acquires fast dynamics and the system does not receive any return from it (Markovian limit). In general, the common FGR has the form expressed in Eq. 7. There, the last factor (N_1) stands for the LDoS of the directly connected states, and by the application of the WBA, it is evaluated in the middle of the band spectrum (in our case, $\varepsilon = 0$).

In this work it is important to remember that the LDoS varies from the semi-infinite chain ($n_\nu = 1$, surface state) to the infinite chain ($n_\nu = -\infty$, bulk state) as follows,

$$N_{1s}(\varepsilon) = \frac{1}{\pi V^2} \left(V^2 - \frac{\varepsilon^2}{4} \right)^{1/2} \Theta[2V - |\varepsilon|], \quad (16)$$

$$N_{1b}(\varepsilon) = \frac{1}{2\pi} \left(V^2 - \frac{\varepsilon^2}{4} \right)^{-1/2} \Theta[2V - |\varepsilon|]. \quad (17)$$

From the previous spectral structures, we stress the presence of van Hove singularities, which play an important role for long time dynamical behavior [28, 42, 69]. Indeed, the critical exponent characterizing the van Hove singularity can be related to the dimensionality of the space where the quantum excitation diffuses. Also, the two different convexities in the LDoS, near the middle of the band spectrum, will be of great relevance in the following discussions.

IV. DECAY RATES: FGR AND BEYOND

In this section we expose the main results of our work, summarized in Table I. The decay rates are presented as function of $V_0^2/\hbar V$, for every case analyzed (Fig. 1) and each approach employed (SP degradation, local LE degradation, WBA-FGR, and SC-FGR).

TABLE I. Degradation rates for all the methods analyzed (Survival Probability and local Loschmidt Echo degradation, Wide Band Approximation, and Self Consistent FGR). The cases are described in Fig. 1. If the system's and bath's time scales are equal, the physical situation is strictly non-Markovian. We point to restore Markovianity in cases where both scales differ by a factor of five.

System	SP degradation rate $\frac{V_0^2}{\hbar V}$	Local LE degradation rate $\frac{V_0^2}{\hbar V}$	WBA $\frac{V_0^2}{\hbar V}$	SC-FGR $\frac{V_0^2}{\hbar V}$
I	2.04 ± 0.05	2.04 ± 0.05	2	2
II	1.00 ± 0.02	1.00 ± 0.02	1	1
III - ($V = V_{AB}$)	0.88 ± 0.05	0.88 ± 0.05	1	0.87
III - ($V = 5V_{AB}$)	1.00 ± 0.02	1.00 ± 0.02	1	0.995
IV - ($V = V_{AB}$)	0.56 ± 0.02	0.56 ± 0.02	0.5	0.577
IV - ($V = 5V_{AB}$)	0.50 ± 0.02	0.50 ± 0.02	0.5	0.502
V	1.16 ± 0.03	1.16 ± 0.03	1	1.15
VI - ($V = V_{AB}$)	1.71 ± 0.04	1.20 ± 0.04	1	1.732(<i>forward</i>) and 0.577 (<i>backward</i>)
VI - ($V = 5V_{AB}$)	1.11 ± 0.03	1.02 ± 0.03	1	1.106(<i>forward</i>) and 0.904 (<i>backward</i>)

The rates predicted in the WBA column of Table I, correspond to the direct evaluation of Eq. 7, i.e.:

$$\frac{1}{\tau_\phi} \simeq \frac{2\pi}{\hbar} V_0^2 N_{1\lambda}(\varepsilon = 0), \quad (18)$$

where λ stands for s (surface, for semi infinite chains) or b (bulk, in the case of infinite chains), in accordance to Eq. 16 and Eq. 17 respectively. Also, the details on the analytic calculation of the rates (SC FGR column, obtained by means of the GF poles) are presented in the Appendix B.

Systems **I** and **II** involves only one site. The difference between them is that **I** has a semi infinite chain acting as environment and **II** has an infinite one. The decay rates for these cases can be directly evaluated within the WBA, and agree exactly with the numerical solutions.

From the cases **III** to **VI**, the system acquires its own time scale (\hbar/V_{AB}). For these cases, we consider two time scales for the environment, as compared to the system's time scale. The first one, in which the time scales are equal ($V = V_{AB}$) and the second in which the environment is "accelerated" by $V = 5V_{AB}$.

Quite obviously, when the environment has the same time scale as the system, the WBA rate does not works at all. However, the rates computed by SP and LE degradation agree with the SC-FGR perfectly (except for the public environment, case **VI**, which will be analyzed below). This last quantity can be interpreted as the LDoS of the bath being evaluated in the exact solution for the eigen-energies of the whole (\mathcal{S} and \mathcal{E}), and not in the middle of the band spectrum (see Fig. 4-a). Indeed, the rate of the SC-FGR is obtained by evaluating the LDoS at the real part of the GF poles.

It is important to notice that the rate obtained for the SC-FGR are *higher* or *lower* than the predicted by the WBA, depending if the bath is *infinite* or *semi-infinite*. We can interpret this result by looking at Fig. 4. Once we evaluate the LDoS in $\text{Re}(\varepsilon_{pole}) \simeq \pm V_{AB}/V$, we observe that the values are lower for the SC-FGR than the WBA in the semi-infinite LDoS, otherwise higher if the infinite LDOS is considered.

At this point, for the two level system, we are able to link the convexity of the bath's LDoS to the observed decay rate. We notice that if the LDoS is *convex*, the exact rates are *greater* than the WBA prediction, but instead if it is *concave*, the rates are *smaller*. In other words, it depends on the shift away from the middle of the band spectrum, moving along the LDoS slope.

In order to point to the strictly Markovian case, where any return from \mathcal{E} to \mathcal{S} is suppressed, we examine accelerated environments. For these cases, all the rates converge to the same value. From Fig. 4-a we can see the convergence of the exact solutions towards the middle of the band spectrum, as long as the condition $V \gg V_{AB}$ is better fulfilled.

So far we have only considered a single and private environment, and in the following cases we address the private-public discussion. As we mentioned before, private baths act over each site individually, and a single public bath acts over two (or eventually more sites) of the same system. This public $\mathcal{S} - \mathcal{E}$ interaction induce new types of correlations, increasing the dynamical complexity of the physical process.

For case **V** we explore the possibility of two private baths (i.e. two infinite environments each one connected to one site). Since here both sites, instead of only one, are affected by the environment, it is expected a double rate compared to the case **IV**. In Table I we found that the simulation results agree with the analytical prediction and again, the rates are greater than the WBA value, which means that we are moving with the exact eigen-energies through a convex LDoS, away from middle of the band.

Finally we analyze a very interesting case, where the system is in presence of a public bath (**VI**). For these cases it is observed that the SP rate differs from the local LE. This behavior shows certain asymmetry between the forward

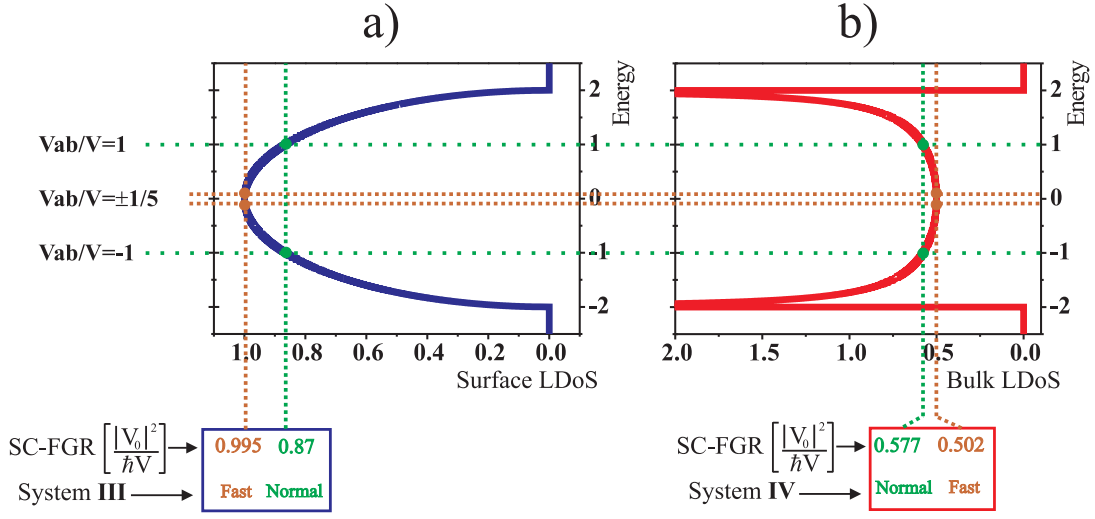


FIG. 4. (Color Online) Local Density of States as function of energy (in units of $1/V_{AB}$ and V_{AB} respectively) for: **a)** Semi-Infinite chain (Surface) and **b)** Infinite chain (Bulk). The horizontal dotted lines are the values V_{AB}/V which stand for the system energies (renormalized with V). The vertical dotted lines together with their numerical values are the LDoS for each system in the normal ($V = V_{AB}$) or the fast ($V = 5V_{AB}$) configuration.

and backward evolutions. Using the SC-FGR approach it can be shown that the imaginary part of the poles depends on the relative value of V_{AB} and V (see Appendix B),

$$\frac{1}{\tau} = \frac{2}{\hbar} \Gamma_0 \simeq \frac{\sqrt{4V^2 - V_{AB}^2}}{2V - V_{AB}} \frac{V_0^2}{\hbar V}. \quad (19)$$

This dependence induces a different decay rate whenever the system evolves forward ($V_{AB} > 0$) or backward ($V_{AB} < 0$). Thus the SP and the local LE are not equivalent (see Table I). It is worth mentioning that the asymmetry (dependence on the relative sign) in the rates for the forward and backward evolutions, arises only when the bath is public.

The analytical prediction for the local LE rate is obtained observing that the total evolution for reversed dynamics is proportional to a product of two exponential evolutions (forward and backward),

$$M_{LE}(T = 2t) \propto \exp\left(-\frac{t}{\tau_f}\right) \exp\left(-\frac{t}{\tau_b}\right) \quad (20)$$

$$= \exp\left[-t \left(\frac{\tau_f + \tau_b}{\tau_f \tau_b}\right)\right] = \exp\left[-T \left(\frac{\tau_f + \tau_b}{2\tau_f \tau_b}\right)\right], \quad (21)$$

where $1/\tau_f$ and $1/\tau_b$ correspond to the forward and backward degradation rates (see also case **VI** in Table I). Eq. 20 shows that the mean rate for a single time-reversed evolution should agree with the LE decay ($1/\tau_{LE} = 1.20 \pm 0.04 V_0^2/\hbar V$). In fact, this is true, since the two SC-FGR rates ($1/\tau_f$ and $1/\tau_b$) yield a mean value $1/\tau = 1.15 V_0^2/\hbar V$. Moreover, and quite obviously, the *forward* rate agrees with the SP decay.

Let us now link the decay process to an appropriate LDoS. As it is clearly shown in Appendix B, we can transform the original model of case **VI** to an equivalent one (see Fig. 5). If a suitable change of basis is applied (basically turning into symmetric and anti symmetric basis), then it is only necessary to analyze two semi infinite linear chains (a particular case treated in Ref. [28, 72]). Since the initial condition has equal weight on both effective chains, the corresponding rates for them have to be added. Further details on the symmetrization transformation are explained in Appendix B.

From the LDoS considered in Fig. 6 we can explain why the rate $1/\tau_f$ is always above the WBA limit, and the $1/\tau_b$ rate is always below it. Moreover, as long as the *forward* rate agrees with the SP decay, this also supports the SP rate being greater than the WBA value.

Once more, we make the bath's dynamics faster, leading to a better applicability of the WBA and the rates converge again to the traditional FGR description (middle of the band spectrum).

Now we briefly analyze the characteristic local LE decay times for a "highly public" bath (See Fig. 7). This case is of interest for studying spin dynamics in ring and ladder like systems (see Ref. [32]).

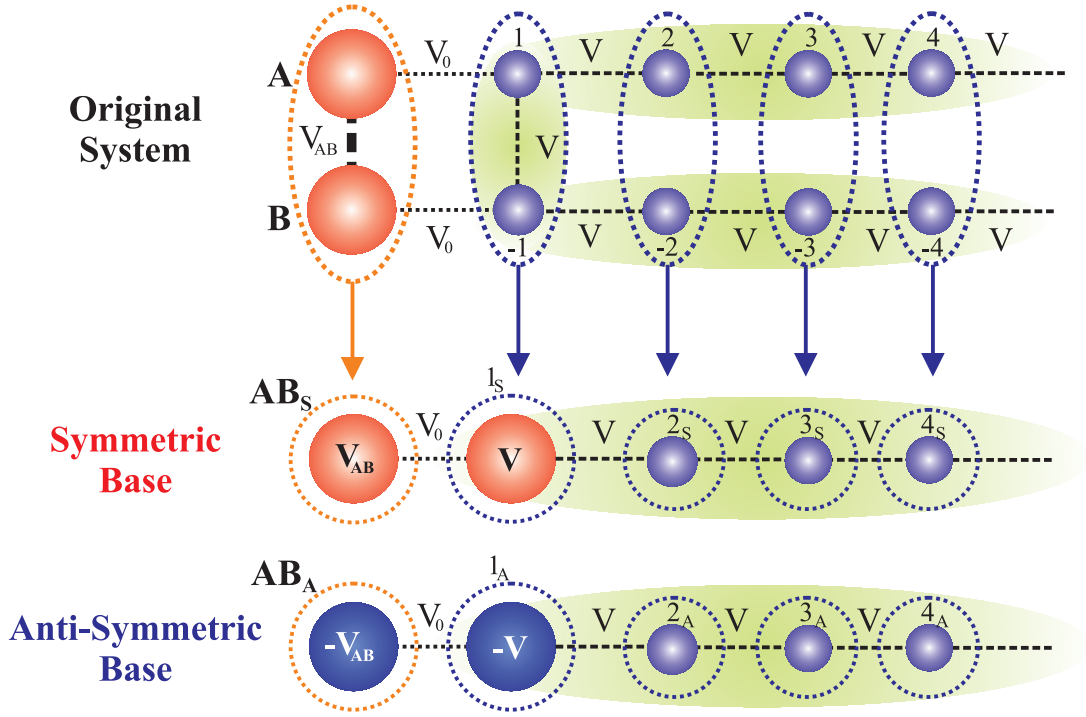


FIG. 5. (Color online). The schematic symmetrization procedure of the 2-sites system interacting with the public environment. The original problem can be cast as two independent semi infinite linear chains.

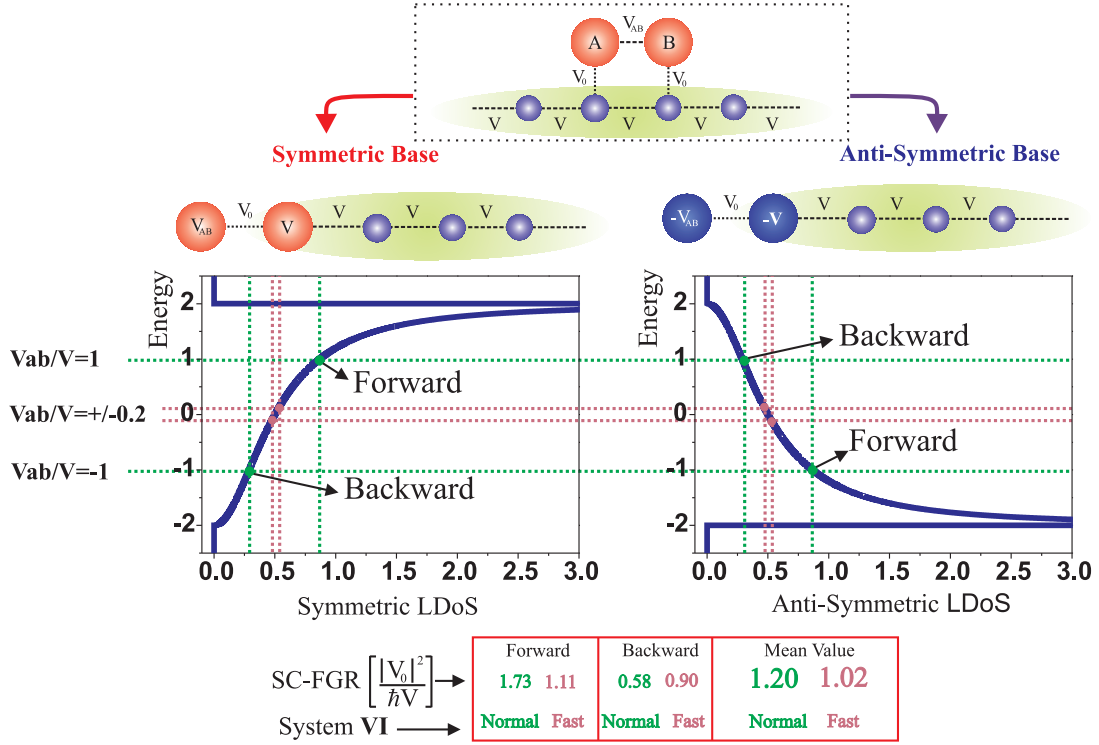


FIG. 6. (Color online) LDoS as function of energy (in units of $1/V_{AB}$ and V_{AB} respectively) for the equivalent problem of the public case, after symmetrization transformation. Forward and backward stages of the evolution are indicated. The horizontal dotted lines are the values V_{AB}/V which stand for the system energies (renormalized to V). The vertical dotted lines together with their numerical values are the LDoS for the system VI in the normal ($V = V_{AB}$) or the fast ($V = 5V_{AB}$) configuration.

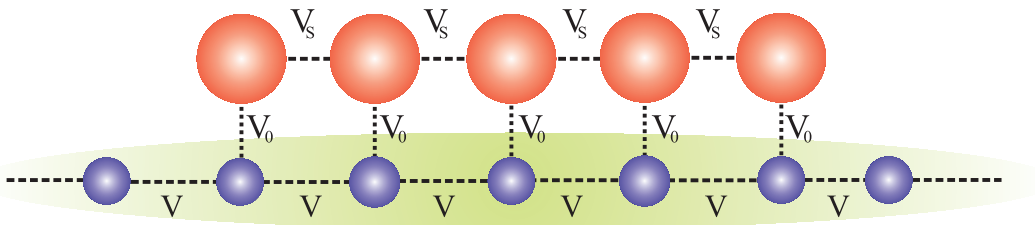


FIG. 7. (Color Online). Fermion model. A five-site system laterally coupled to an infinite chain.

In this system we will consider three different relation for time scales: $V = V_s$, $V = 5V_s$ and $V = 8.75V_s$ (we also assume $V \gg V_0$). For these cases the decay rates (local LE degradation rate measured in units of $V_0^2/\hbar V$) computed by the numerical solution are (2.66 ± 0.07) , (1.54 ± 0.05) and (1.16 ± 0.04) , respectively. Therefore, we observe that the first two results do not match with that expected by WBA. Moreover, as we have seen before, the convexity of the bulk LDoS, induce bigger values. By setting $V = 8.75V_s$ (approximately one order of magnitude of difference) we are near the WBA validity and thus nearly reproduce the expected result: an energy independent rate, of value $1.00 V_0^2/\hbar V$, in accordance to Eq. 18. We stress here that the strong sensibility on the relation between time scales, is enhanced by a highly public $\mathcal{S} - \mathcal{E}$ interaction.

V. FURTHER DISCUSSIONS AND CONCLUSIONS

Traditionally, the first approach to evaluate decay rates is the FGR based on an underlying WBA. We have shown several variations of a simple SWAP gate interacting with an environment (or several ones) where this scheme is not as good as one might assume. This failure, which can be understood as non-Markovianity, is due to two contributions (which should not be considered as well separated effects).

First, if the WBA limit ($V \gg V_{AB}$) is not well fulfilled, then it is quite obvious that the energy independent rate will not be representative as it would oversimplify the decay process. When the system's time scale becomes comparable to that of the environment (i.e. $V_{AB} \simeq V$, non-Markovian situation), the decay rate departs from the usual FGR approximation evaluated at single energy level. Depending on the bath's spectral structure (LDoS) the actual rate can be greater or lower. We have shown that if the LDoS is a convex function of the energy, then any shift away from the middle of the band spectrum will produce a greater decay rate. But if the LDoS is a concave energy function, the rate would be lower. In general, we have seen that dynamical complexity (understood as how much the decay departs from the WBA validity) arises when the time scales of the system, the environment and the $\mathcal{S} - \mathcal{E}$ interactions, are commensurable.

Second, when the dynamics is non-Markovian due to similar time scales, the possibility of interaction through the environment becomes appreciable. In a public bath, the correlations generated by the multiple connections between different parts of the system and the bath, are more effective to depart the physical process away from the WBA validity, for a given relation of time scales. In general this leads to too subtle correlations to be treated in spectral models for the bath which here becomes quite natural through the use of specific Hamiltonian models of the environment.

In order to address the question on the private and public nature of the $\mathcal{S} - \mathcal{E}$ interaction, we confront the cases of *two independent baths* (case **V**) and *one common bath* (case **VI**). In cases where $\mathcal{S} - \mathcal{E}$ interaction is private there is no dependence of the rate on the relative sign of V and V_{AB} . On the other hand, if the $\mathcal{S} - \mathcal{E}$ interaction is public, the forward and backward evolution will change the decay rates and will produce a mean value for the local LE decoherence rate. It is important to stress here that we are comparing cases where \mathcal{S} and \mathcal{E} have similar time scales. In this condition, it is observed that decay rates for the public case are greater than for the private. In this sense we interpret (at least for this cases) that the private bath is less harmful than a public one. Strictly speaking, this is a consequence of moving along the LDoS in the *effective* FGR (see Figs. 4 and 6). A public scenario produces an enhancement in the alteration of the FGR away from the WBA limit, as compared to the private one. As a matter of fact, private bath is less efficient for correlated memory-like returns to the system. As it has been previously stated in a general sense, and based on complete formal grounds, the feedback of information from \mathcal{E} to \mathcal{S} is the central issue for quantifying a non-Markovian bath [73].

On the other hand, we have shown how Markovianity is restored by changing the relation between \mathcal{S} and \mathcal{E} time scales. In fact, for all the cases treated in this work, we have found that once we move towards the WBA limit (represented by a bath dynamics 5 times faster than the system's), the effects of a public or private bath are no longer relevant. For both cases the environment is fast enough to wash out all the memory effects, since any inner excitation

is rapidly spread. At this point the rate for both situations become equal and agree with the one predicted by the common FGR. This means that when the system's and the bath's time scales are well differentiated (specifically when the bath's is very short as compared to the system's), then the public-private reservoir discussion becomes irrelevant.

In many physical situations, when addressing 1-D and 1-D⁺ systems (see, for example [32]), a coupled environment behaves with a convex LDoS. Therefore, memory effects and complexity in the structure of the $\mathcal{S} - \mathcal{E}$ interaction produce an enhancement of the coherent dynamics degradation. Additionally, we stress here the wider "spectral exploration" of the Loschmidt Echo as compared to the Survival Probability (a difference clearly shown in the public $\mathcal{S} - \mathcal{E}$ interaction case, where the global LE rate is a mean value of two non symmetric processes).

Even though we do not claim full generality for the results discussed here, there are some interesting universal issues to remark. The use of the Wide Band Approximation (simple FGR) can easily lead to quantitative and qualitative errors if the time scales and the physical structure of \mathcal{S} and \mathcal{E} are similar. Furthermore, the way they are coupled to each other (*public* or *private*), plays a fundamental role. In general, dynamical complexity grows when those characteristic times are similar and when there is no privacy in the $\mathcal{S} - \mathcal{E}$ interaction.

ACKNOWLEDGMENTS

We acknowledge financial support from ANPCyT, SeCyT-UNC, MinCyT-Cor, CONICET. This work was benefited from fruitful discussions with P. R. Levstein and R. Bustos-Marín. The authors acknowledge F. Rojo and F. Pastawski for useful comments on the manuscript.

Appendix A: Excitation dynamics in 1-d systems and the Spin-Fermion mapping

In previous sections we developed a scheme that could be used to treat spin polarization dynamics [31, 33], under certain assumptions. In that sense, the well-known mapping between spins and fermions [51] has been used for formulating the spin problem in terms of the non-equilibrium Keldysh formalism [30, 52, 74]. We briefly present here the Spin-Fermion mapping, and how the tight binding models discussed along the present article arise.

A simple case that can be treated in this context is a linear chain of M spins in an external magnetic field. They interact with their nearest neighbors through XY coupling:

$$\hat{H} = \sum_{n=0}^{M-1} \hbar\Omega_n \hat{S}_n^z - \sum_{n=0}^{M-2} J_{n+1,n} [\hat{S}_{n+1}^x \hat{S}_n^x + \hat{S}_{n+1}^y \hat{S}_n^y] \quad (\text{A1})$$

$$= \sum_{n=0}^{M-1} \hbar\Omega_n \hat{S}_n^z - \sum_{n=0}^{M-2} \frac{1}{2} J_{n+1,n} [\hat{S}_{n+1}^+ \hat{S}_n^- + \hat{S}_{n+1}^- \hat{S}_n^+], \quad (\text{A2})$$

where \hat{S}_n^\pm are the rising and lowering operators $\hat{S}_n^\pm = \hat{S}_n^x \pm i\hat{S}_n^y$. The dynamics of the M -spin system, evolving under the Hamiltonian \hat{H} , is usually described by means of the two site spin correlation function,

$$P_{f,i}(t) = \frac{\langle \Psi_{eq} | \hat{S}_f^z(t) \hat{S}_i^z(t_0) | \Psi_{eq} \rangle}{\langle \Psi_{eq} | \hat{S}_f^z(t_0) \hat{S}_i^z(t_0) | \Psi_{eq} \rangle}. \quad (\text{A3})$$

The quantity of Eq. A3 gives the amount of local polarization in the z component at time t on the f th site, provided that the system was, at time t_0 , in its equilibrium state with a spin up added at i th site. Also, $\hat{S}_f^z(t) = e^{i\hat{H}t} \hat{S}_f^z e^{-i\hat{H}t}$ is the spin operator in the Heisenberg representation and $|\Psi_{eq}\rangle = \sum_N a_N |\Psi_{eq}^{(N)}\rangle$ is the thermodynamical many-body equilibrium state constructed by adding states with different number N of spins up with appropriate statistical weights and random phases.

The Jordan-Wigner transformation (JWT) links spin and fermion operators at each site, by the following relation:

$$\hat{S}_n^+ = \hat{c}_n^\dagger \exp \left[i\pi \sum_{m=1}^{n-1} \hat{c}_m^\dagger \hat{c}_m \right] \quad (\text{A4})$$

where $\hat{c}_m^\dagger, \hat{c}_m$ are the canonical fermionic operators. The use of the JWT on the Hamiltonian A2 yields:

$$\hat{H} = \sum_{n=0}^{M-1} \varepsilon_n (\hat{c}_n^\dagger \hat{c}_n - \frac{1}{2}) - \sum_{n=0}^{M-2} V_{n+1,n} [\hat{c}_{n+1}^\dagger \hat{c}_n + \hat{c}_n^\dagger \hat{c}_{n+1}], \quad (\text{A5})$$

where $\varepsilon_n \equiv \hbar\Omega_n$ are the site energies and $V_{n+1,n} \equiv \frac{1}{2}J_{n+1,n}$ are the hoppings. Due to the short range interaction (first neighbors), after the application of the JWT, the only non-zero coupling terms between spins are proportional to $\hat{c}_{n+1}^\dagger \hat{c}_n = \hat{S}_{n+1}^+ \hat{S}_n^-$. Each subspace with $\binom{M}{N}$ states of spin projection $\langle \sum_{n=1}^M \hat{S}_n^z \rangle = N - M/2$ is now a subspace with N non-interacting fermions. The eigenfunctions $|\Psi_\gamma^{(N)}\rangle$ are expressed as a single Slater determinant built up with the single particle wave functions φ_α of energy ε_α . Under these circumstances, and setting $|i\rangle \equiv \hat{c}_i^\dagger |\emptyset\rangle$ (with $|\emptyset\rangle$ the fermion vacuum), Eq. A3 reduces to:

$$\begin{aligned} P_{f,i}(t) &= \left| \langle f | \exp \left[-i\hat{H}t/\hbar \right] | i \rangle \Theta(t) \right|^2 \\ &= \hbar^2 |G_{f,i}^R(t)|^2, \end{aligned} \quad (\text{A6})$$

where $G_{f,i}^R(t)$ is the retarded Green's function for a single fermion that connects sites f and i .

While similar steps lead to description of excitations in Double Quantum (DQ) Hamiltonian [53–56]:

$$\hat{H}_{DQ} = \sum_{n=0}^{M-2} \frac{J_{n+1,n}}{2} [\hat{S}_{n+1}^+ \hat{S}_n^+ + \hat{S}_{n+1}^- \hat{S}_n^-], \quad (\text{A7})$$

those will not be detailed here. The fundamental issue is the underlying one-body dynamics, which for the DQ Hamiltonian is revealed by a unitary transformation $\hat{H}_{DQ} = U^\dagger \hat{H}_{XY} U$ [54, 56] that links it to an XY Hamiltonian.

Hence, for one dimensional (1-D) chains of spins with first neighbors XY or DQ interactions, and in the high temperature regime, the dynamics of an excitation (either an injected local polarization or multiple quantum coherence) is completely equivalent to the evolution of a single particle wave function, ruled by a tight-binding Hamiltonian. Therefore, it turns out that the analysis of Hamiltonians like the one in Eq. A5, can be casted for treating and studying several effects in spin chains [75] (a typical scenario in QIP).

Appendix B: Green's Function Poles.

Here we present the detailed analytical derivation of the GF poles and further approximations. The results from this appendix have been summarized in the Table I showed in Sec. IV.

The first model under consideration (Fig. 1-I) is given by one site coupled to a semi-infinite chain. In this case the GF pole results purely imaginary,

$$\varepsilon_{pole} = -i \frac{V_0^2}{\sqrt{V^2 - V_0^2}}. \quad (\text{B1})$$

Even though this is indeed the exact solution, we span it for $V_0^2/V \ll 1$ and obtain:

$$\varepsilon_{pole} \simeq \frac{V_0^2}{V}. \quad (\text{B2})$$

Thus the theoretical decay rate for this model can be expressed as:

$$\frac{1}{\tau} = \frac{2}{\hbar} \Gamma_0 = \frac{2}{\hbar} \text{Im}(\varepsilon_{pole}) \simeq \frac{2}{\hbar} \frac{V_0^2}{V}. \quad (\text{B3})$$

If we change the environment to an infinite chain (Fig. 1-II) the pole is,

$$\varepsilon_{pole} = -i \left(2V^2 \left(1 - \sqrt{\frac{V_0^4}{4V^4} + 1} \right) \right)^{1/2} \simeq -i \frac{V_0^2}{2V} \quad (\text{B4})$$

The case **III**, which corresponds to two sites coupled to a semi-infinite chain, has been solved previously in Ref. [42],

$$\varepsilon_{pole}^2 = \frac{V_{AB}^2 (2V^2 - V_0^2) - V_0^4 \pm V_0^2 \sqrt{(V_{AB}^2 + V_0^2)^2 - 4V_{AB}^2 V^2}}{2(V^2 - V_0^2)}. \quad (\text{B5})$$

Using the solutions of Eq. (26) and (27) in Ref. [42], we can directly evaluate the real and imaginary parts of the poles,

$$\begin{aligned} \Delta_0 &= \pm \left(\frac{V_{AB}^2 (2V^2 - V_0^2) - V_0^4}{2(V^2 - V_0^2)} + \Gamma_0^2 \right)^{1/2} \\ &\simeq \pm V_{AB} \left(1 - \frac{1}{4V} \frac{V_0^2}{V} \right) \end{aligned} \quad (\text{B6})$$

$$\begin{aligned} \Gamma_0 &= \left(\frac{V_0^4 - V_{AB}^2 (2V^2 - V_0^2)}{4(V^2 - V_0^2)} + \sqrt{\frac{V^2 V_{AB}^4}{4(V^2 - V_0^2)}} \right)^{1/2} \\ &\simeq -\frac{1}{4} \frac{\sqrt{4V^2 - V_{AB}^2}}{V} \frac{V_0^2}{V}. \end{aligned} \quad (\text{B7})$$

Now, we change slightly the geometry of these systems and consider again an infinite chain as environment instead the semi-infinite. For these cases we will write only the first non trivial terms of their Taylor expansion instead of the full solution. For the model of Fig. 1-**IV**, the solution is:

$$\Delta_0 \simeq \pm V_{AB} + O\left(\frac{V_0^4}{V^4}\right) \quad (\text{B8})$$

$$\Gamma_0 \simeq -\frac{1}{2} \frac{V}{\sqrt{4V^2 - V_{AB}^2}} \frac{V_0^2}{V} + O\left(\frac{V_0^4}{V^4}\right). \quad (\text{B9})$$

The next case (Fig. 1-**V**) is a two-site system coupled to two private baths. In this case, the solution is,

$$\Delta_0 \simeq \pm V_{AB} + O\left(\frac{V_0^4}{V^4}\right) \quad (\text{B10})$$

$$\Gamma_0 \simeq -\frac{V}{\sqrt{4V^2 - V_{AB}^2}} \frac{V_0^2}{V} + O\left(\frac{V_0^4}{V^4}\right). \quad (\text{B11})$$

At this point we observe that the imaginary part for the case **V** is twice of the system **IV**. This behavior is consistent with the count of the “number” of private baths connected to the system, and the proportion affected by those private baths.

Finally, for the case of Fig. 1-**VI**, the model involves a two-site system coupled to a common bath. For this case the solution is expressed in the following form,

$$\Delta_0 \simeq \pm \left(V_{AB} - \frac{1}{2} \frac{V_0^2}{V} \right) + O\left(\frac{V_0^4}{V^4}\right) \quad (\text{B12})$$

$$\Gamma_0 \simeq -\frac{\sqrt{4V^2 - V_{AB}^2}}{4V - 2V_{AB}} \frac{V_0^2}{V} + O\left(\frac{V_0^4}{V^4}\right). \quad (\text{B13})$$

Notice that the imaginary part of the pole is linear in V_{AB} in a sign dependent manner (in contrast to previous cases). This linearity translate into a different value for Γ_0 depending on the sign of V_{AB} . As a matter of fact, the

local LE indeed relies on the change of sign to revert the dynamics. To understand the physics below this difference we have to identify the LDoS involved in the decay process. Accordingly, we symmetrize the basis, thus dimerizing the system, as shown in Fig. 5 (i.e. we take pairs of site states and map them into symmetric and anti symmetric states.) Therefore the tight binding Hamiltonian for this case is mapped to the form of Eq. B14.

$$\begin{aligned}
\hat{H} &= \begin{pmatrix} & |A\rangle & |B\rangle & |1\rangle & |-1\rangle & |2\rangle & |-2\rangle & \dots & \dots \\ \langle A| & & V_{AB} & & & V_0 & & & \\ \langle B| & V_{AB} & & & & V_0 & & & \\ \langle 1| & & & V_0 & & V & V & & \\ \langle -1| & & & & V & & & V & \\ \langle 2| & & & & & V & & \ddots & \\ \langle -2| & & & & & & V & & \ddots \\ \vdots & & & & & & & \ddots & \\ \vdots & & & & & & & & \ddots \end{pmatrix} \\
\rightarrow \hat{H}' &= \begin{pmatrix} & \dots & |2_S\rangle & |1_S\rangle & |AB_S\rangle & |AB_A\rangle & |1_A\rangle & |2_A\rangle & \dots \\ \vdots & & & & & & & & \\ \langle 2_S| & & \ddots & & & & & & \\ \langle 1_S| & & & V & & & & & \\ \langle AB_S| & & & & V & & & & \\ \langle AB_A| & & & & & V_0 & & & \\ \langle 1_A| & & & & & & -V_{AB} & V_0 & \\ \langle 2_A| & & & & & & & & V_0 & -V & V \\ \vdots & & & & & & & & & & V & \ddots \\ \vdots & & & & & & & & & & & \ddots \end{pmatrix} \tag{B14}
\end{aligned}$$

where $|n_S\rangle = (|n\rangle + |-n\rangle)/\sqrt{2}$, $|n_A\rangle = (|n\rangle - |-n\rangle)/\sqrt{2}$, $n = 1, 2, 3..$ and $|AB_S\rangle = (|A\rangle + |B\rangle)/\sqrt{2}$, $|AB_A\rangle = (|A\rangle - |B\rangle)/\sqrt{2}$. From the Hamiltonian \hat{H}' (Eq. B14) it is easy to identify the splitting of the original problem into two semi infinite tight binding chains, with only the first two site energies non zero. This problem has been previously addressed in Refs. [28] and [72] and we recall the LDoS computed there. Thus in Fig. 6 we identify the energy excitation on the spectral structure of the environment, which is relevant during the decay process.

-
- [1] C. H. Bennett and D. P. DiVincenzo, *Nature* **404**, 247 (2000).
 - [2] W. H. Zurek, *Rev. Mod. Phys.* **75**, 715 (2003).
 - [3] I. T. Vink, K. C. Nowack, F. H. L. Koppens, J. Danon, Y. V. Nazarov, and L. M. K. Vandersypen, *Nature Phys.* **5**, 764 (2009), arXiv:0902.2659 [cond-mat.mes-hall].
 - [4] H. Bluhm, S. Foletti, I. Neder, M. Rudner, D. Mahalu, V. Umansky, and A. Yacoby, *Nature Phys.* **7**, 109 (2011).
 - [5] H. O. H. Churchill, A. J. Bestwick, J. W. Harlow, F. Kuemmeth, D. Marcos, C. H. Stwertka, S. K. Watson, and C. M. Marcus, *Nature Phys.* **5**, 321 (2009), arXiv:0811.3236 [cond-mat.mes-hall].
 - [6] C. Latta, A. Högele, Y. Zhao, A. N. Vamivakas, P. Maletinsky, M. Kroner, J. Dreiser, I. Carusotto, A. Badolato, D. Schuh, W. Wegscheider, M. Atature, and A. Imamoglu, *Nature Phys.* **5**, 758 (2009), arXiv:0904.4767 [cond-mat.mes-hall].
 - [7] A. Morello, J. J. Pla, F. A. Zwanenburg, K. W. Chan, K. Y. Tan, H. Huebl, M. Möttönen, C. D. Nugroho, C. Yang, J. A. van Donkelaar, A. D. C. Alves, D. N. Jamieson, C. C. Escott, L. C. L. Hollenberg, R. G. Clark, and A. S. Dzurak, *Nature* **467**, 687 (2010), arXiv:1003.2679 [cond-mat.mes-hall].
 - [8] N. Mizuochi, P. Neumann, F. Rempp, J. Beck, V. Jacques, P. Siyushev, K. Nakamura, D. J. Twitchen, H. Watanabe, S. Yamasaki, F. Jelezko, and J. Wrachtrup, *Phys. Rev. B* **80**, 041201 (2009), arXiv:0811.4731 [quant-ph].
 - [9] R. Hanson, V. V. Dobrovitski, A. E. Feiguin, O. Gywat, and D. D. Awschalom, *Science* **320**, 352 (2008).
 - [10] L. Childress, M. V. G. Dutt, J. M. Taylor, A. S. Zibrov, F. Jelezko, J. Wrachtrup, P. R. Hemmer, and M. D. Lukin, *Science* **314**, 281 (2006).

- [11] L. M. K. Vandersypen, M. Steffen, G. Breyta, C. S. Yannoni, M. H. Sherwood, and I. L. Chuang, *Nature* **414**, 883 (2001).
- [12] C. Ramanathan, N. Boulant, Z. Chen, D. G. Cory, I. Chuang, and M. Steffen, in *Experimental Aspects of Quantum Computing*, edited by H. O. Everitt (Springer US, 2005) pp. 15–44.
- [13] G. A. Alvarez, E. P. Danieli, P. R. Levstein, and H. M. Pastawski, *J. Chem. Phys.* **124**, 194507 (2006).
- [14] R. L. Kosut, A. Shabani, and D. A. Lidar, *Phys. Rev. Lett.* **100**, 020502 (2008).
- [15] E. Knill and R. Laflamme, *Phys. Rev. A* **55**, 900 (1997).
- [16] C. A. Ryan, J. S. Hodges, and D. G. Cory, *Phys. Rev. Lett.* **105**, 200402 (2010).
- [17] T. D. Ladd, F. Jelezko, R. Laflamme, Y. Nakamura, C. Monroe, and J. L. O'Brien, *Nature* **464**, 45 (2010), arXiv:1009.2267 [quant-ph].
- [18] C. L. Degen, *Appl. Phys. Lett.* **92**, 243111 (2008).
- [19] J. M. Taylor, P. Cappellaro, L. Childress, L. Jiang, D. Budker, P. R. Hemmer, A. Yacoby, R. Walsworth, and M. D. Lukin, *Nature Phys.* **4**, 810 (2008), arXiv:0805.1367 [cond-mat.mes-hall].
- [20] P. W. Anderson, *J. Phys. Soc. Japan.* **9**, 316 (1954), its description of the line collapse and the further exchange narrowing in a Markovian environment can be considered as a first evidence of a dynamical quantum phase transition.
- [21] I. Rotter, *J. Phys. A* **42**, 153001 (2009).
- [22] H. M. Pastawski, *Physica B* **398**, 278 (2007).
- [23] P. W. Anderson, *Science* **177**, 393 (1972).
- [24] S. Chakravarty and A. J. Leggett, *Phys. Rev. Lett.* **52**, 5 (1984).
- [25] E. Danieli, G. Álvarez, P. Levstein, and H. Pastawski, *Solid State Commun.* **141**, 422 (2007).
- [26] G. A. Álvarez, E. P. Danieli, P. R. Levstein, and H. M. Pastawski, *Phys. Rev. A* **75**, 062116 (2007).
- [27] J. M. Taylor, A. Imamoglu, and M. D. Lukin, *Phys. Rev. Lett.* **91**, 246802 (2003).
- [28] E. Rufeil-Fiori and H. Pastawski, *Chem. Phys. Lett* **420**, 35 (2006).
- [29] L. Müller, A. Kumar, T. Baumann, and R. R. Ernst, *Phys. Rev. Lett.* **32**, 1402 (1974).
- [30] E. P. Danieli, H. M. Pastawski, and G. A. Álvarez, *Chem. Phys. Lett.* **402**, 88 (2005).
- [31] Z. L. Mádi, B. Brutscher, T. Schulte-Herbrüggen, R. Brüschweiler, and R. R. Ernst, *Chem. Phys. Lett.* **268**, 300 (1997).
- [32] G. A. Álvarez, E. P. Danieli, P. R. Levstein, and H. M. Pastawski, *Phys. Rev. A* **82**, 012310 (2010).
- [33] H. M. Pastawski, P. R. Levstein, and G. Usaj, *Phys. Rev. Lett.* **75**, 4310 (1995).
- [34] H. M. Pastawski, G. Usaj, and P. R. Levstein, *Chem. Phys. Lett.* **261**, 329 (1996).
- [35] R. A. Jalabert and H. M. Pastawski, *Phys. Rev. Lett.* **86**, 2490 (2001).
- [36] H. M. Pastawski, P. R. Levstein, G. Usaj, J. Raya, and J. Hirschinger, *Physica A* **283**, 166 (2000).
- [37] P. R. Levstein, G. Usaj, and H. M. Pastawski, *J. Chem. Phys.* **108**, 2718 (1998).
- [38] M. F. Andersen, A. Kaplan, T. Grünzweig, and N. Davidson, *Phys. Rev. Lett.* **97**, 104102 (2006).
- [39] R. Schäfer, H.-J. Stöckmann, T. Gorin, and T. H. Seligman, *Phys. Rev. Lett.* **95**, 184102 (2005).
- [40] T. Gorin, T. Prosen, T. H. Seligman, and M. Znidaric, *Phys. Rep.* **435**, 33 (2006).
- [41] P. Jacquod and C. Petitjean, *Adv. Phys* **58**, 67 (2009).
- [42] A. D. Dente, R. A. Bustos-Marín, and H. M. Pastawski, *Phys. Rev. A* **78**, 062116 (2008).
- [43] C. Cohen-Tannoudji, G. Grynberg, and J. Dupont-Roc, *Atom-Photon Interactions: Basic Processes and Applications* (Wiley, New York, 1992) in Ch.I defines the Rabi oscillation as that occurring between two degenerate states under the action of a constant perturbation. In quantum optics, it is now usual to call Rabi oscillations to those appearing when two non-degenerate levels are irradiated at resonance. This last reduces to the first when described in the rotating frame.
- [44] E. Rufeil-Fiori and H. M. Pastawski, *Braz. J. Phys.* **36**, 844 (2006), arXiv:quant-ph/0604069.
- [45] G. M. Palma, K.-A. Suominen, and A. K. Ekert, *Proc. R. Soc. A* **452**, 567 (1996).
- [46] H. Breuer and F. Petruccione, *The theory of open quantum systems* (Oxford University Press, 2007).
- [47] P. Zanardi and M. Rasetti, *Phys. Rev. Lett.* **79**, 3306 (1997).
- [48] A. Buchleitner, A. R. R. Carvalho, and F. Mintert, *Acta Phys. Pol. A* **112**, 575 (2007).
- [49] J. P. Paz and A. J. Roncaglia, *Phys. Rev. A* **79**, 032102 (2009).
- [50] M. Hor-Meyll, A. Auyuanet, C. V. S. Borges, A. Aragão, J. A. O. Huguenin, A. Z. Khoury, and L. Davidovich, *Phys. Rev. A* **80**, 042327 (2009).
- [51] E. Lieb, T. Schultz, and D. Mattis, *Ann. Phys. (N.Y.)* **16**, 407 (1961).
- [52] E. P. Danieli, H. M. Pastawski, and P. R. Levstein, *Chem. Phys. Lett.* **384**, 306 (2004).
- [53] E. B. Fel'dman and S. Lacelle, *J. Chem. Phys.* **107**, 7067 (1997).
- [54] S. Doronin, I. Maksimov, and E. Feldman, *J. Exp. Theor. Phys.* **91**, 597 (2000).
- [55] P. Cappellaro, C. Ramanathan, and D. G. Cory, *Phys. Rev. A* **76**, 032317 (2007).
- [56] E. Rufeil-Fiori, C. M. Sánchez, F. Y. Oliva, H. M. Pastawski, and P. R. Levstein, *Phys. Rev. A* **79**, 032324 (2009).
- [57] E. Economou, *Green's functions in Quantum Physics* (Springer, Berlin, 1983).
- [58] R. A. Bustos-Marín, E. A. Coronado, and H. M. Pastawski, *Phys. Rev. B* **82**, 035434 (2010).
- [59] H. L. Calvo and H. M. Pastawski, *Europhys. Lett.* **89**, 60002 (2010).
- [60] B. L. Hu, J. P. Paz, and Y. Zhang, *Phys. Rev. D* **45**, 2843 (1992).
- [61] B. Bartels, ArXiv e-prints (2011), arXiv:1106.1371 [cond-mat.stat-mech].
- [62] F. M. Cucchietti, D. A. R. Dalvit, J. P. Paz, and W. H. Zurek, *Phys. Rev. Lett.* **91**, 210403 (2003).
- [63] Note: Notice that the systems we are considering do not have enough complexity to warrant a perturbation independent (i.e. Lyapunov) decoherence rate.
- [64] G.-L. Ingold, *Coherent Evolution in Noisy Environments*, Lecture Notes in Physics, Vol. 611 (Springer-Verlag, Berlin, 2002)

p. 1.

- [65] H. M. Pastawski and E. Medina, *Rev. Mex. Fis.* **47**, 1 (2001), arXiv:cond-mat/0103219.
- [66] P. Facchi and S. Pascazio, *La regola d'oro di Fermi* (Bibliopolis, Napoli, 1999).
- [67] P. Facchi and S. Pascazio, *Phys. A* **271**, 133 (1999).
- [68] P. Facchi and S. Pascazio, *Phys. Lett. A* **241**, 139 (1998).
- [69] S. A. Khal'fin, *Sov. Phys. JETP* **6**, 1053 (1958).
- [70] L. Fonda, G. C. Ghirardi, and A. Rimini, *Rep. Prog. Phys.* **41**, 587 (1978).
- [71] G. García-Calderón, J. L. Mateos, and M. Moshinsky, *Phys. Rev. Lett.* **74**, 337 (1995).
- [72] E. Rufeil-Fiori and H. Pastawski, *Physica B* **404**, 2812 (2009).
- [73] H.-P. Breuer, E.-M. Laine, and J. Piilo, *Phys. Rev. Lett.* **103**, 210401 (2009).
- [74] L. V. Keldysh, *Zh. Eksp. Teor. Fiz.* **47**, 1515 (1964), *sov. Phys. JEPT* **20**, 1018 (1965).
- [75] P. Cappellaro, L. Viola, and C. Ramanathan, *Phys. Rev. A* **83**, 032304 (2011), arXiv:1011.0736 [quant-ph].